JOURNAL OF MULTIFUNCTIONAL MATERIALS & PHOTOSCIENCE
5(1), June 2014, pp. 77-99

Research Progress in Bismuth-based Photocatalysts with π-conjugate Molecule and Their Photocatalysis Properties

Jian Yang[1], Feng-Jun Zhang[1,2*], Fa-Zhi Xie[1], Wen-Jie Xie[1] and Han-Mei Hu[2]

[1]*Anhui Key Laboratory of Advanced Building Materials, Anhui Jianzhu University, Hefei Anhui P. R. China, 230022*
[2]*Key Laboratory of Functional Molecule Design and Interface Process, Anhui Jianzhu University Hefei Anhui, P. R. China, 230601*

Abstract: Bismuth based photocatalyst is a new material with layered structure, which facilitates the separation of photoproduction holes and electrons. And they possess high photocatalytic activation and chemical stability in specific reaction condition. BiOX (X=Cl, Br, I), Bi_2WO_6, $Bi_2O_2CO_3$, $BiVO_4$ and Bi_2MoO_6 all have absorption edge of visible light. π-conjugated molecules (CNTs, graphene, PANI, g-C_3N_4) have been doped into Bi based photocatalysts on accout of being broaden the range of light absorption and reducing the recombination of hole and electron. These π-conjugated molecules forming a good heterojunction with each other have better photocatalytic efficiency than P25 (commercial TiO_2) under visible light at the same conditions and the effect of π-conjugated molecules are synergistic efficient. Bismuth-based heterojunction with π-conjugate molecule is a promising research direction as a visible light photocatalyst.

Keywords: Bismuth based photocatalyst, π-conjugated molecules, photocatalytic properties

1. Introduction

Recently, Bismuth based photocatalysts have catched much attention own to suitable band gap, layer structure and appropriate absorption. For instance, BiOX (Cl, Br, I) [1-3], Bi_2WO_6 [4-5], $Bi_2O_2CO_3$ [6], $BiVO_4$ [7] and Bi_2MoO_6 [8-9] had been demonstrated that they are response to visible light sensitively. However, these Bi based materials also have their own defects. For example, they can not sufficiently use solar energy because of their narrow edge of photoabsorption. Sole photocatalysts often exhibit high possibilities of recombination rate of the charge carries.

Conjugated molecule is one kind of chemical compounds that contain carbon-carbon double bond and a single bond and a double bond arrange alternately, such as carbon nanotubes (CNTs), graphene, polyaniline (PANI) and graphitic carbon nitride (g-C_3N_4). Usually, they reveal proper performance in absorption spectrum, refractive index, bond

Corresponding author: zhang-fengjun@hotmail.com*

length and heat of hydrogenation. At the same time, graphene, PANI can directly be used as photocatalysts. Surprisingly, g-C_3N_4 can be applied to photocatalytic water splitting and organic pollutant [10-11].

Both theoretical and experimental researches have revealed that proper doping will improve photocatalytic efficiency dramatically in many kinds of photocatalysts [12-14]. Combining with π-conjugated molecules such as CNTs, graphene, PANI, g-C_3N_4 forming heterojunction is expected to enhance the photocatalytic efficiency and reduce the recombination of photoinduced hole and electron due to these conjugated molecules containing conjugated double bonds whose electrons can be easily excited to LUMO under visible light irrigation and then transfer into CB of semiconductors leading to organic pollutants mineralization. Herein, this review will focus on research progress of the preparation, characterization and photocatalytic properties of bismuth based photocatalysts with π-conjugated molecules such as CNTs, graphene, PANI, g-C_3N_4.

2. CNTs-BiOX (X=Cl, Br, I) heterojunctions

CNTs were firstly discovered in 1991 which were considered as one of the most potential CDI electrode materials. CNTs possess special properties such as high conductivity, excellent chemical stability [15-17]. CNTs could perform as electrons accepter by trapping electrons transferred from semiconductor photocatalyst [18]. So, Bi based-CNTs composite should show great photocatalytic properties. Graphene has drawn much attention because of its single layer of carbon atoms densely packed in a honeycomb crystal lattice recently [19-20]. It possesses huge surface area (ca.2630m^2/g), chemical stabilities and the most attractive property allows it to have strong π-π interactions with the aromatic moieties present in most dyes [21].

BiOX (X=Cl, Br, I) as a kind of novel photocatalysts, has a special lamellar structure and inner static field which is benefit for the separation of photoelectrons and photoholes dramatically. They are all V-VII ternary compound which crystallizes in the tetragonal matlockite structure [22]. The band gap of BiOX diminishes step by step from Cl to I. Eg of BiOCl, BiOBr and BiOI is approximate 3.21ev [23], 2.8ev [24] and 1.87ev [25], representatively. BiOBr and BiOI possess excellent visible light response because of comparably narrow band gap which can absorb the visible light directly. Nevertheless, BiOCl can only be excited by UV light.

The multi-walled carbon nanotubes have aroused much interest for their special structures and electrical properties [26]. Recently, efforts have been devoted to synthesize CNTs/BiOI, CNTs/BiOBr, Ag/AgX-CNTs (X= Cl, Br, I) nanocomposite [27], Titania-Coated Carbon Nanotubes (CNTs) [28] and CNTs/TiO_2 [29]. In these composites, CNTs plays an important role in the photocatalytic process, which promotes the charge carries separation and reduces the recombination.

2.1. CNTs/BiOI

CNTs/BiOI was prepared by EG-assisted solvothermal method at 160! for 12h with $Bi(NO_3)_3{\cdot}5H_2O$ and KI regard as the raw material [30]. Fig. 1 showed that BiOI-1%CNTs

was microsphere with a polyporous surface. The picture of TEM can be seen the BiOI consisited of solid structured spheres and irregular nanoplates can be seen on the surface of BiOI microspheres. Fig. 2 shows that the prepared BiOI-CNTs composites exhibit strong photocatalytic activation using AOII (acid orange II) as organic pollutant under visible light. The efficiency of AOII degradation increased with the increase of CNTs amount from 0.5 to 1.0% significantly. The photocatalytic degradation of AOII using BiOI-CNTs composites under visible light was completed within 180 min. Based on Fig. 3, a possible pathway for degradation of AOII was proposed. They thought the degradation process of AOII included the involvement of ·OH active radical which attacked the AOII to degrade CO_2 and H_2O ultimately.

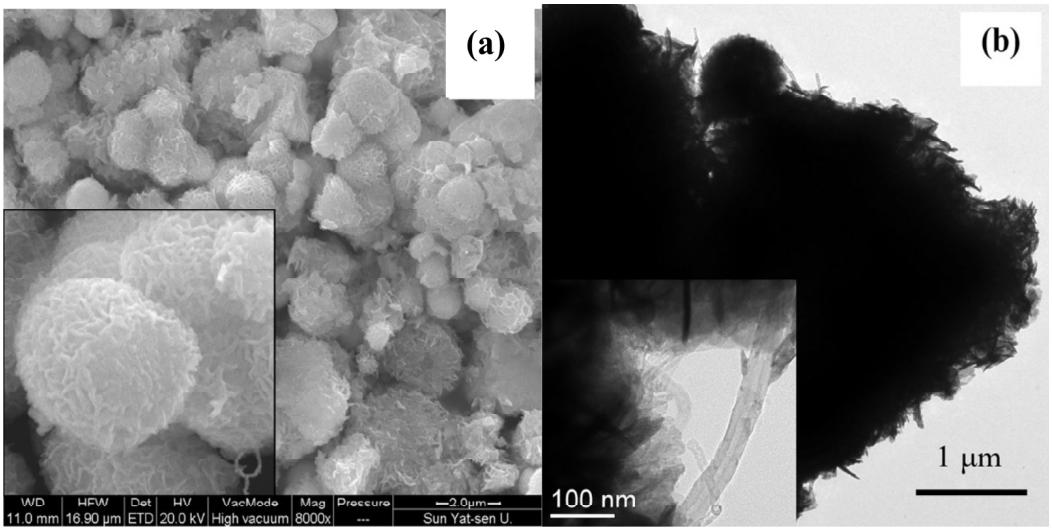

Figure 1: SEM (a) and TEM (b) patterns of BiOI-1% MCNTs.

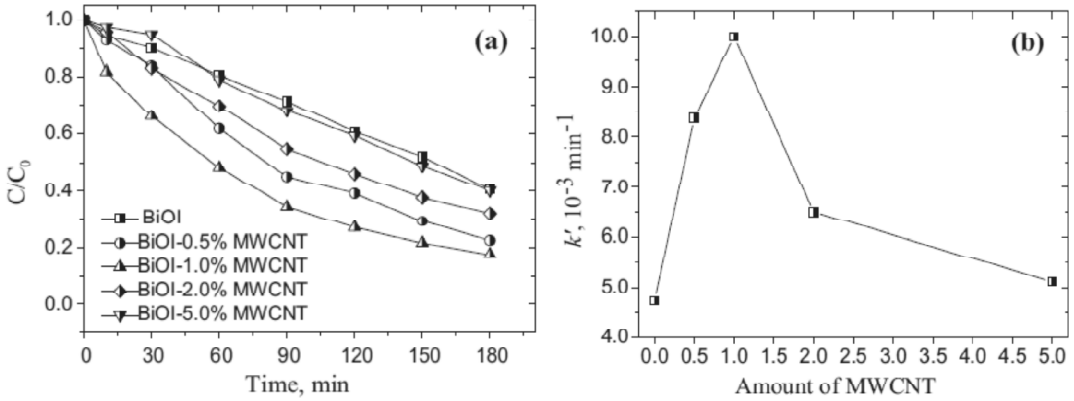

Figure 2: (a) Effect of doped CNTs amount in BiOI-CNTs composites on degradation efficiency of AOII under visible light irradiation, and (b) values of k as a function of doped CNTs amount in BiOI-CNTs composites.

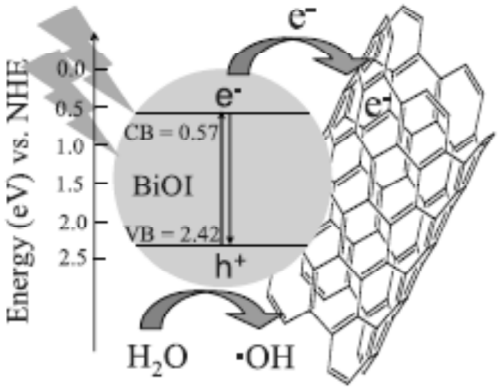

Figure 3: Schematic illustration of the proposed photocatalytic mechanism of BiOI-CNTs under visible light.

2.2. CNTs/ BiOBr

Li huaming and coworkers had synthesized novel flower-like BiOBr/CNTs composite photocatalysts through a one-pot EG-assisted solvothermal process in the presence of reactable ionic liquid 1-hexadecyl-3-methylimidazolium bromide as the Br source [31]. SEM pattern (Fig. 4a) showed that a large number of CNTs attached to the surface of CNTs/BiOBr microsphere. TEM pattern (Fig. 4b) further conformed that the composites were spheres-like structures. The absorption peak around 1630 cm^{-1} corresponded to the bending vibrations of O–H, which was ascribed to the water adsorbed. The absorption band at 510cm^{-1} was ascribed to the Bi–O stretching mode. No characteristic absorption peak of the ionic liquids was found in the FT-IR spectra (Fig. 5a). As can be seen from Fig. 5b, the 0.05wt% BiOBr/CNTs composite exhibited the highest photocatalytic activity. Only 31.3% RhB was photodegraded by pure BiOBr after irradiation for 30 min while the 0.05wt% BiOBr/CNTs photodegraded 77.4%.

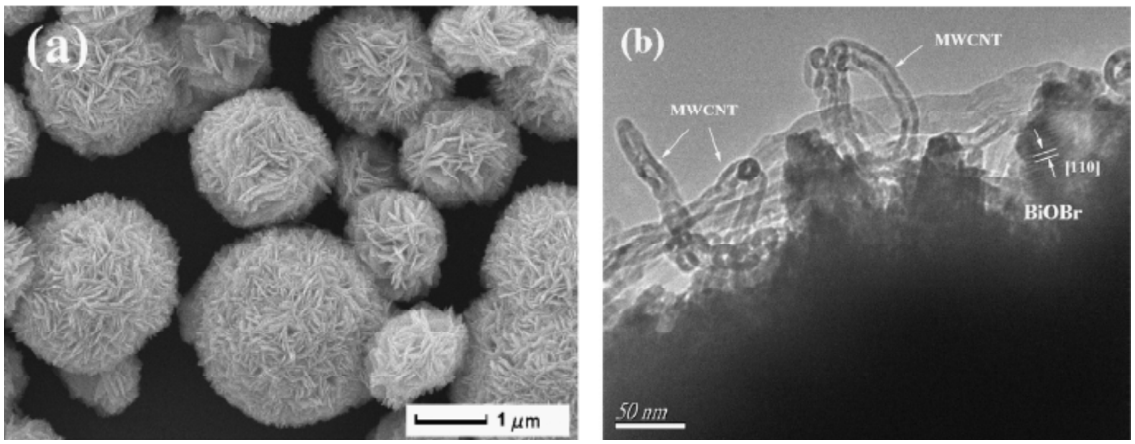

Figure 4: SEM (a) and TEM (b) images of the 0.05 wt% CNTs/BiOBr microspheres structures.

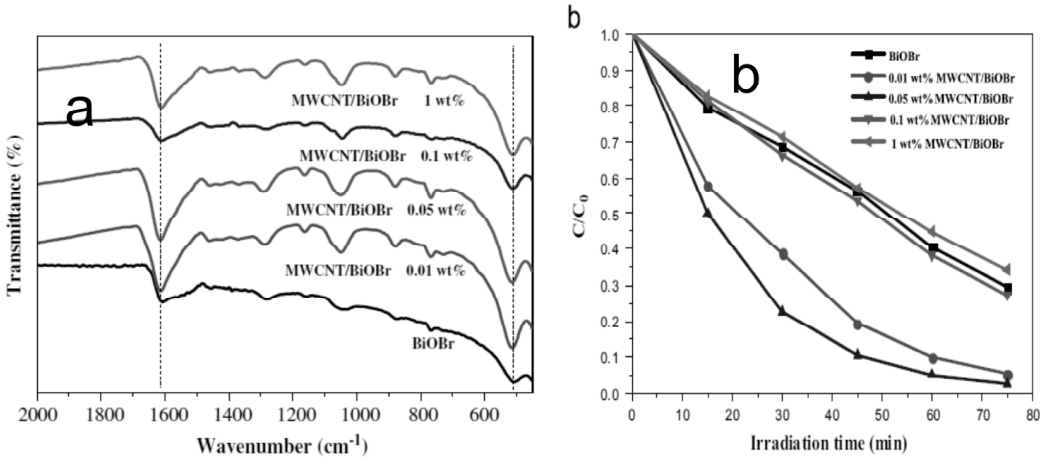

Figure 5: (a) Transient photocurrent response for the pure BiOBr and CNTs/BiOBr. (b) Temporal UV–vis absorption spectral changes during the photocatalytic degradation of RhB in aqueous solution in the presence of CNTs/BiOBr.

3. Graphene-Bi based Composite

Graphene, consisting of a monolayer of carbon atoms arranged in a 2D honeycomb lattice, shows excellent mechanical, thermal, optical and electrical properties and has aroused wide interest in photocatalysis. It possesses p conjugated electrons and outstanding electrons transportation. As a result, it can assist the charge carries in the surface of Bi based semiconductors in transferring quickly reducing the possibilities of the recombination rate [32-33].

3.1. Graphene/BiOBr$_{0.2}$I$_{0.8}$

Liu hong and coworkers had synthesized a series of graphene sheets grafted three-dimensional BiOBr$_{0.2}$I$_{0.8}$ BiOBr$_{0.2}$I$_{0.8}$ microspheres with different graphene contents by a simple one-step solvothermal method [34]. The BiOBr$_{0.2}$I$_{0.8}$ microspheres were composed of numerous nanoplates with a thickness of about 10 nm and dispersed uniformly on the surface of graphene (Fig. 6). The assembled BiOBr$_{0.2}$I$_{0.8}$/graphene composites exhibited excellent photocatalytic activity in the degradation of rhodamine B (RhB) and phenol under visible light irradiation (e”420 nm). The optimal graphene content was found to be 10.0 wt% and the corresponding photocatalytic activity in degradation of RhB and phenol was 3.19 and 3.27 times that of pure BiOBr$_{0.2}$I$_{0.8}$, respectively. The enhanced photocatalytic activity could be attributed to more effective charge transportations and separations, larger specific surface areas and the increased light absorption.

They had proposed the mechanism in photocatalytic process which firstly should be ascribed to the efficient charge separation and transfer (Fig. 7). Under visible light illumination, the electrons on the VB of BiOBr$_{0.2}$I$_{0.8}$ are excited to the CB, creating holes in the VB. Then the photogenerated electrons can transfer from the CB of BiOBr$_{0.2}$I$_{0.8}$ to the graphene because of the high work function of graphene. This results in the formation of

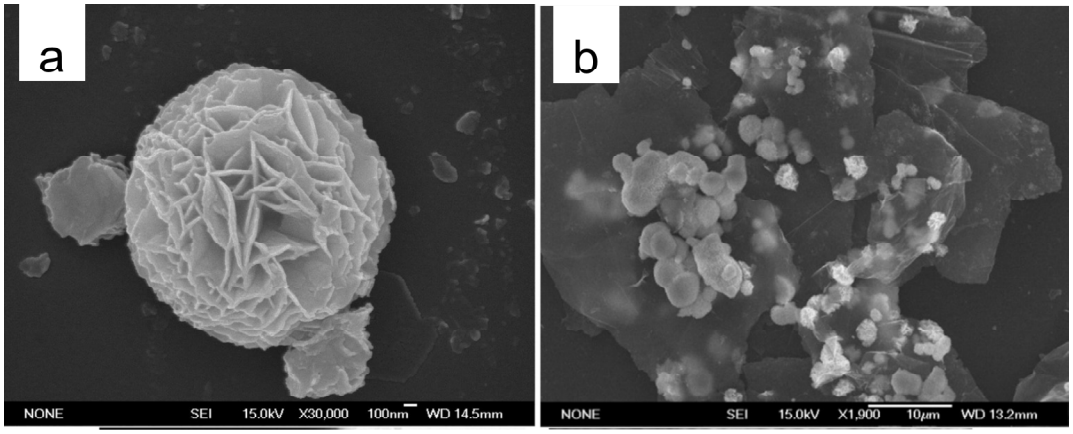

Figure 6: SEM images of $BiOBr_{0.2}I_{0.8}$ (a) and $BiOBr_{0.2}I_{0.8}$/graphene (b).

Schottky barrier at the interface between $BiOBr_{0.2}I_{0.8}$ and graphene, which improves the charge separation. In the photocatalytic process, the photogenerated electrons accumulated on the surface of graphene had good fluidity and could be transferred to surface-absorbed oxygen rapidly to form activated $O_2^{\bullet -}$. On the other hand, holes accumulated at the VB of $BiOBr_{0.2}I_{0.8}$ could also react with surface adsorbed H_2O or OH^- to give rise to hydroxyl radical •OH. Both these radicals are strong oxidants that can effectively oxidize organic molecules to water and carbon dioxide.

Ji guangbin and co-workers also synthesized graphene/BiOBr composite following hydrothermal reaction between graphene oxide and BiOBr [35]. The results achieved demonstrated that the presence of graphene on the surface of BiOBr significantly improved the photocatalytic activity, under visible light irradiation, owing to the low isoelectric

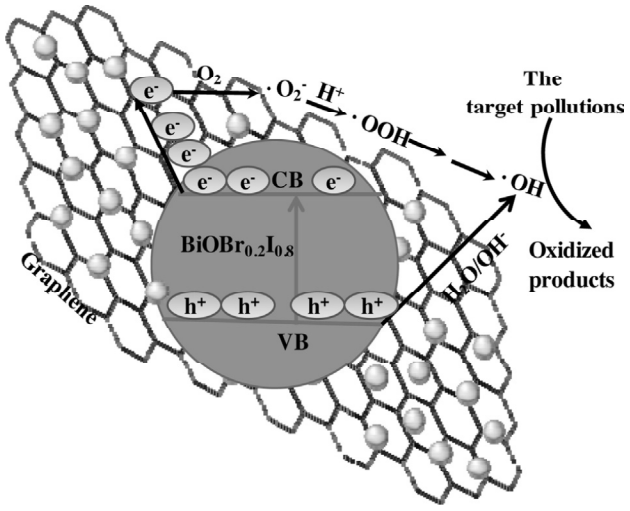

Figure 7: Photocatalytic mechanism of $BiOBr_{0.2}I_{0.8}$/graphene composites.

characteristics of graphene and better interfacial electron transfer between BiOBr and graphene. Yang bai and co-workers used one-pot synthesis to synthesize graphene–BiOBr nanosheets composite [36]. They thought that the graphene can change the conduction band (CB) and valence band (VB) of BiOBr toward enhanced photocatalytic activity for reactive oxygen species (ROS) generation than that of BiOBr under visible-light irradiation (Fig. 8).

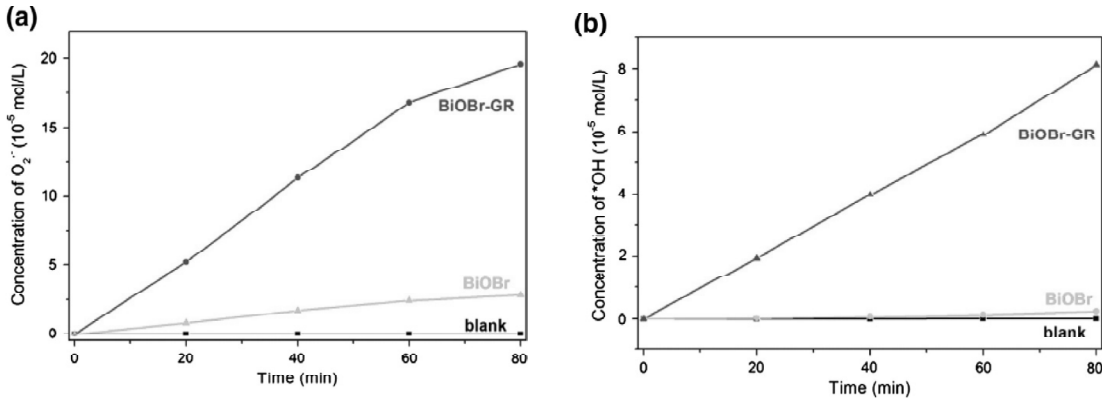

Figure 8: (a) $O_2^{\bullet-}$ and (b) •OH generation over BiOBr and BiOBr–RG under visible-light irradiation.

3.2. Graphene-$BiVO_4$

Recently, sun qianghui [37] reported that a simple and efficient route for the controllable synthesis of dumbbell-shaped $BiVO_4$ hierarchical structures at a large scale with uniform size and shape distributions was demonstrated, where the as-synthesized $BiVO_4$ products were then incorporated with prepared reduced graphene oxide (RGO)sheets to form dumbbell-shaped $BiVO_4$/RGO composites. Wang xin and co-workers prepared a $BiVO_4$–graphene photocatalyst by a facile one-step hydrothermal method [38]. The representative SEM images of the prepared $BiVO_4$–graphene were shown in Fig. 9. It can be seen from the micrographs that the obtained products are of unique dumbbell-shaped architectures and uniform size distributions by sun qianghui, whereas the almost transparent graphene sheets are decorated by leaf-like $BiVO_4$ lamellas with an average particles size of 1-1.3um and a thickness of about 15 nm. It was hardly ever reported in the literature.

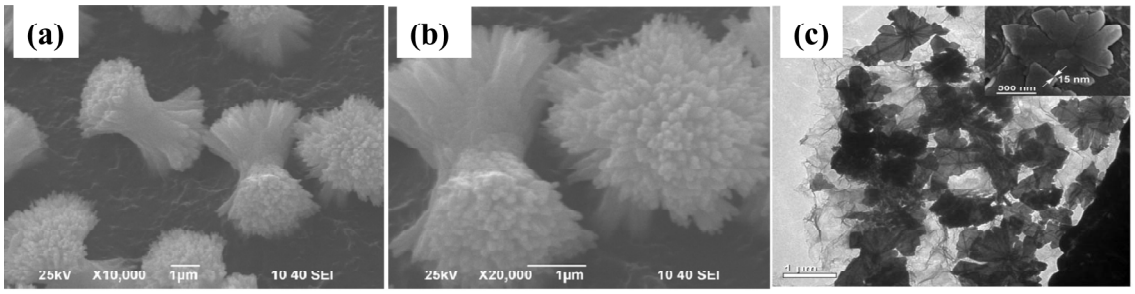

Figure 9: SEM images of the prepared dumbbell-shaped $BiVO_4$ (a, b). Typical TEM and SEM (insert) image of $BiVO_4$–graphene, with leaves-like $BiVO_4$ sheets loading on the surface of graphene (c).

It can be observed from Fig. 10 that after 6 h reaction, the degradation efficiency of RhB solution (with an initial concentration of 7.5 mg L^{-1}) reaches 71% and 96.5% in the presence of pure dumbbell-shaped $BiVO_4$ and BG-3, respectively. Complete decolorization of RhB in the presence of BG-3 is achieved within 8 h, whilst only reaching 96% even after 10 h irradiation by using pure dumbbell-shaped $BiVO_4$. For $BiVO_4$–graphene, the photodegradation rates of MB reached 89% after irradiation for only 180 min and reached up to 99% after irradiation for 300 min, which demonstrated that almost all the MB molecules in the solution had been decomposed. In contrast, the photodegradation rate of MB over pure $BiVO_4$ was 60% after irradiation for 360 min under the same conditions

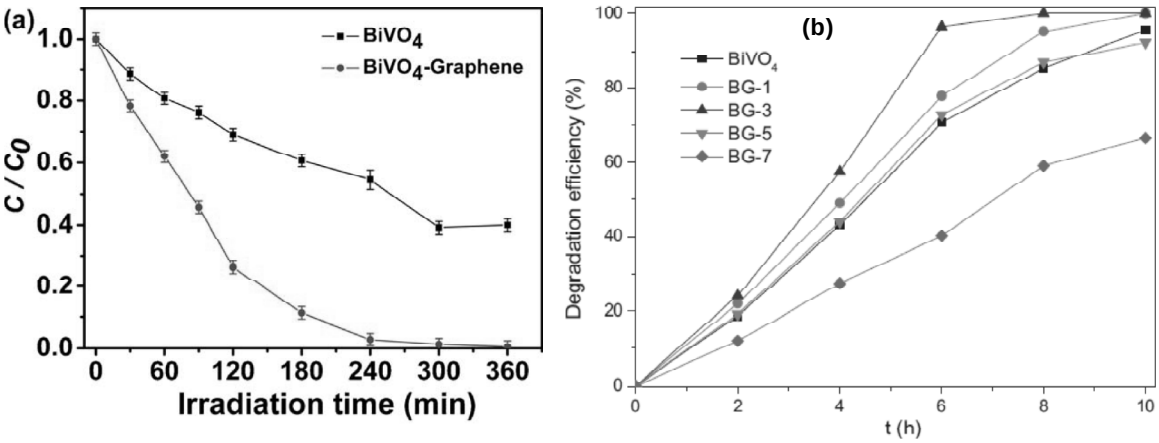

Figure 10: (a) Photocatalytic degradation rates of MB using $BiVO_4$–graphene and pure$BiVO_4$ photocatalysts (b) The comparison of the degradation efficiency of RhB (7.5 mg L^{-1}) in aqueous solution by using pure dumbbell-shaped $BiVO_4$ architectures and $BiVO_4$/RGO composites as photocatalysts under natural sunlight irradiation.

3.3. Graphene–BiOI

Liu Hong reported a series of chemically bonded Bismuth oxyiodide (BiOI)–graphene (GR) nanocomposites have been synthesized by a facile one-step hydrothermal method [39]. In the Raman spectrum of graphene oxide (Fig. 11a), two typical bands of graphene oxide can be found at 1350 (D band) and 1607 cm^{-1} (G band). The G band is generally assigned to the E_{2g} phonon of sp^2 bonds of carbon atoms. For the BiOI–GR composites, all the Raman bands for tetragonal BiOI can be found. Significantly, the two characteristic peaks at about 1347 cm^{-1} (D band) and 1598 cm^{-1} (G band) for the graphitized structures are observed in the Raman spectroscopy of BiOI–GR composites. For GO (Fig. 11b), the characteristic peaks of oxygen-containing functional groups are revealed by the bands at 1060, 1228, 1396, and 1726 cm^{-1}, which correspond to C-O-C stretching vibrations, the C-OH stretching peak, the O-H deformation of the C-OH groups, the C=O stretching vibrations of the -COOH group, respectively. The peak at 1631 cm^{-1} can be assigned to the skeletal vibrations of unoxidized graphitic domains. The wide band at 3440 cm^{-1} should originate from the absorption of water or O-H groups. For BiOI–GR composites, the

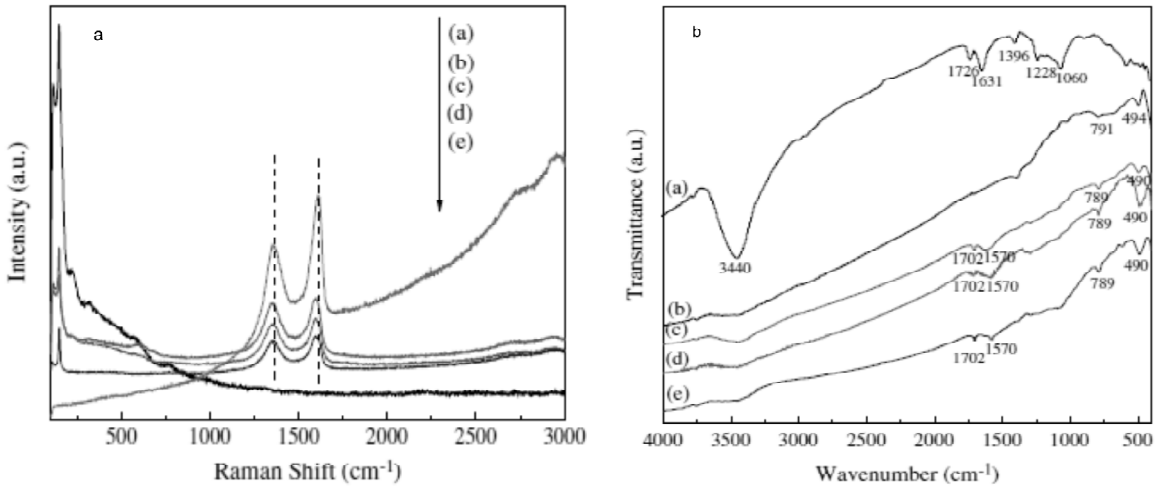

Figure 11: (a) Raman spectra of GO, BiOI and BiOI–GR composites: (a) GO, (b) BG3.0, (c) BG2.0, (d) BG1.0, and (e) BiOI. (b) FT-IR spectra of GO, BiOI and BiOI–GR composites: (a) GO, (b) BiOI, (c) BG1.0, (d) BG2.0, and (e) BG3.0.

characteristic features of GO are almost disappeared, revealing that these oxygen-containing functional groups were almost removed.

It is well known that the generation and separation of the photoinduced electron–hole pairs are the key factors to influence a photocatalytic reaction. Under visible excitation, the electron of BiOI can be promoted from the valence band to the conduction band, leaving behind a hole in the valence band. Then, the electron transfers to graphene. In the photocatalytic process, the photogenerated electrons accumulated on the surface of graphene had good fluidity and could be transferred to surface-absorbed oxygen rapidly to form activated $\cdot O^-_2$. The activated $\cdot O^-_2$ further produces ·OH via a series of reaction with H^+. This step is the photoreduction process. On the other hand, holes accumulated at the

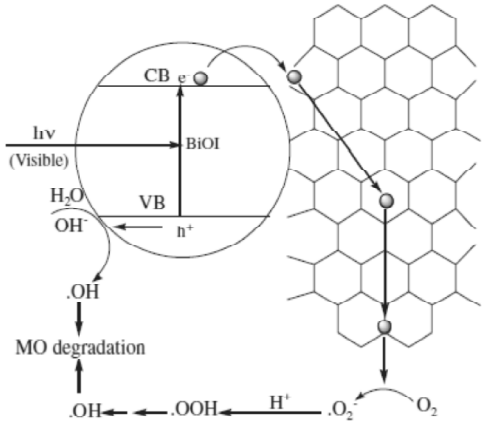

Figure 12: Photocatalytic mechanism of BiOI–GR composites.

valence band of BiOI could also react with H_2O to give rise to hydroxyl radical ·OH, which is the photooxidation process. Both the photoreduction and photooxidation step generate ·OH which is responsible for the degradation of pollutant.

Two-dimensional (2D) coupling of BiOBr nanosheets with graphene (Ge) and graphene oxide (GO) nanosheets were synthesized by a simple and low-cost method at room temperature by dong fang and co-workers [40]. The obtained BiOBr–Ge and BiOBr–GO nanocomposites exhibit significantly enhanced photocatalytic activity for the degradation of RhB and removal of NO under visible light irradiation, in contrast with the pure BiOBr.

3.4. Graphene-Bi_2WO_6

A series of reduced graphene oxide (RGO) modified Bi_2WO_6 nanocomposites were synthesized by hydrothermal method [41]. The results indicated that the RGO could be used as structure-directing agent in the process of formation of the RGO/Bi_2WO_6 nanocomposites (Fig. 13).

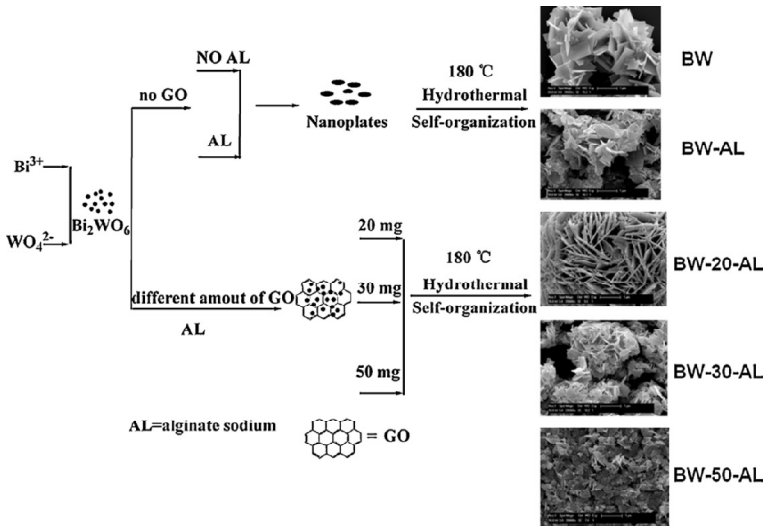

Figure 13: Formation process for different products obtained under different conditions.

Other workers reported that reduced graphene oxide/Bi_2WO_6 (RGO–Bi_2WO_6) composite photocatalysts were prepared by a simple one-pot method. Namely, the reduction of graphene oxide and the growth of Bi_2WO_6 crystal occurred simultaneously in one single process [42]. The results were such that composite photocatalysts showed much higher photocatalytic activity than did Bi_2WO_6 for MB degradation under visible light. Zhang kan and co-workers reported Bi_2WO_6 incorporated on graphene sheets using a facile refluxing method to improve its photocatalytic performance[43]. Remarkable three times enhancement in photodegradation of Rh.B was observed on Bi_2WO_6/graphene composite compared with pure Bi_2WO_6 under visible light irradiation. This improvement was attributed to the longer electron lifetime of excited Bi_2WO_6 as the electrons even if

holes were injected to graphene instantly at the site of generation, leading to a maximized charge separation. This demonstrated that the graphene as supporter could provide an effective way for enhancing photocatalytic performance of semiconductor photocatalysts by acting as charge transfer channel (Fig. 14).

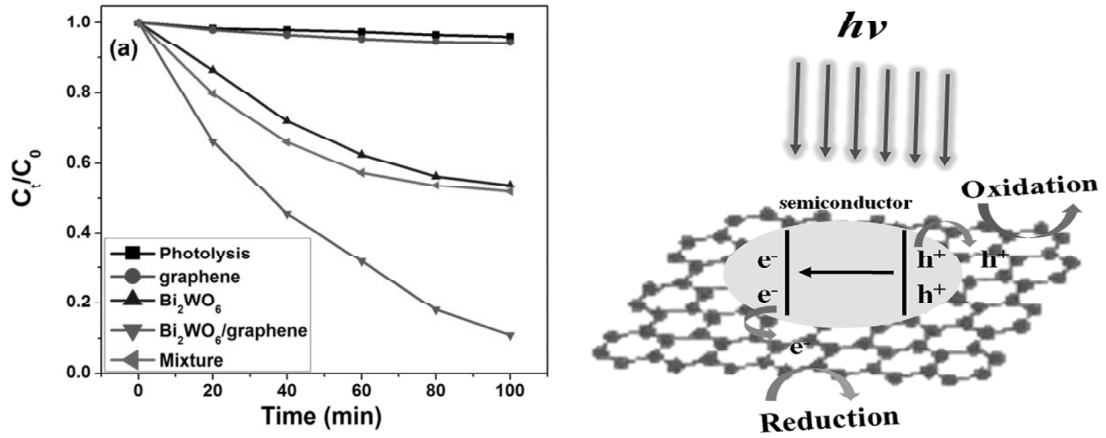

Figure 14: (a) Photocatalytic degradation of Rh.B under visible light. (b) Proposed mechanism of light irradiating to graphene based semiconductor photocatalysts.

4. PANI-Bi based Composite

Conducting polymers polyaniline (PANI) as a conducting polymer with an extended π-conjugated electron system has recently showed great promises due to its high absorption coefûcients in the visible-light range and high mobility of charge carriers [44]. PANI composed of benzenoid and quinonoid units with the delocalized conjugated structures has several redox states which have extensive interesting properties [45]. PANI is more valuable in practice for ease of commercial scale production.

4.1. PANI-BiOCl

Photocatalyst BiOCl modified by polyaniline (PANI/BiOCl) was synthesized via a facile chemisorptions method [46]. The results showed that the PANI increased absorption intensity and absorption bands of the pure BiOCl. Photodegradation of methyl orange (MO) on the samples were investigated under visible light irradiation and 7 wt% PANI/BiOCl composite showed the highest photocatalytic activity. As shown in Fig. 15(a), it could be seen clearly that the BiOCl was dominated with surface smooth plates and the thickness is about 50 nm. In Fig. 12(b), the7 wt% PANI/BiOCl was mainly composed of many plates with small particles, which dispersion on the surface of plates.

Both pure BiOCl and PANI showed very low photocatalytic activity under visible light irradiation, but their composites have shown the excellent photocatalytic performance on the degradation of MO. On the one hand, the various types of dyes have different the molecular structures, which result in different degradation mechanisms. In the

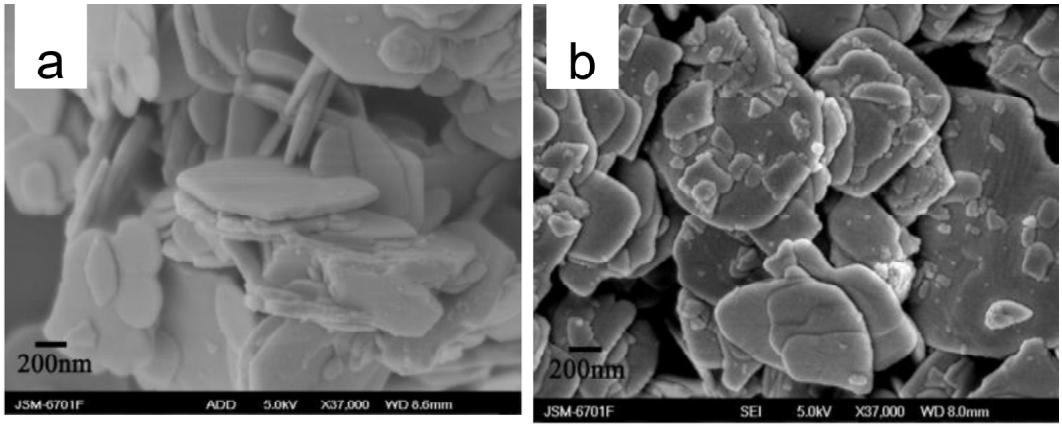

Figure 15:SEM images of (a) BiOCl (b) 7 wt% PANI/BiOCl.

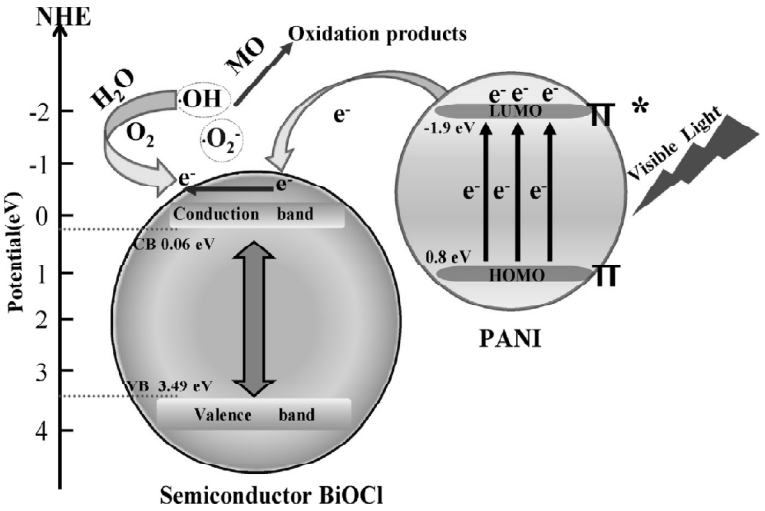

Figure 16: Schematic illustration of the proposed photocatalytic mechanism of PANI/BiOCl under visible light irradiation.

photocatalysis process of a semiconductor for dye degradation, the oxidative species forming over catalyst surface decompose the dye via a pathway from intermediates to the final carbon dioxide (CO_2) and some inorganic products (SO_4^{2-},NO_3^-, NH_4^+). On the other hand, it can be found that BiOCl can not be excited under visible light irradiation because it could only absorb UV light. Thanks to PANI can absorb visible light to induce π–π* transition, delivering the excited-state electrons of HOMO orbital to LUMO orbital. Since the CBM of BiOCl and π* orbital of PANI match well in energy level and have chemical bond interaction, which can cause synergistic effect. Based on the synergistic effect, the excited-state electrons could easily inject into the CBM of BiOCl and subsequently transfer to the surface to react with water and oxygen to yield hydroxyl and superoxide radicals, which would oxidize the MO.

4.2. PANI / Bi_2WO_6

Bi_2WO_6 photocatalyst film prepared by a facile chemical bath deposition (CBD) method was modified by polyaniline (PANI) through in situ polymerization of vapor phase aniline [47]. The annealed CBD films were dipped into an ammonium persulfate (APS) solution. 2% (v/v) of concentrated HCl was added to the oxidant solution in order to obtain the acid doping PANI coating layer which is conductive. Excess APS solution was wiped off. The films were then transferred into a reactor which was heated by hot plate at 40 °C to make the monomer solution of aniline evaporate. The monomer vapors polymerized when they came in contact with the APS-coated films, producing a thin PANI coating, doped with H^+ ions. The polymerization time was set as 1 h. Afterwards, the obtained film was collected and rinsed with anhydrous ethanol and deionized water and then oven-dried at 60 °C (Fig. 17).

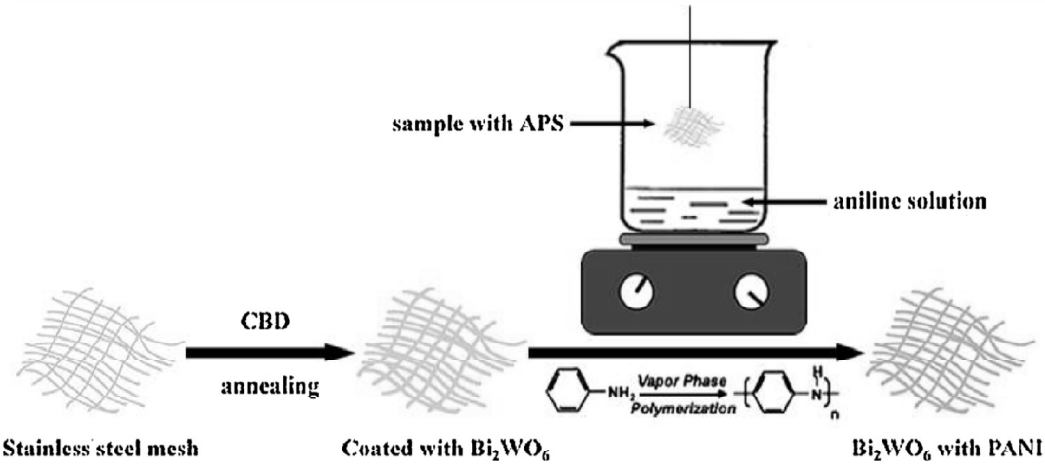

Figure 17: The process of in situ polymerization of PANI on Bi_2WO_6 film by CBD method

From Fig. 18 of SEM pattern, at lower concentration, Bi_2O_3 particles were obtainedand they were smaller and closely packed into larger agglomerates. They tended to aggregate on bent parts of stainless steel wire with high surface energy instead of uniformly coat on the whole part of the wire. While at higher concentration, the size distribution of Bi_2WO_6 particles was uniform consisting of spheres with a diameter of 400–500 nm. Higher concentration favored to form larger particles and thicker coating layers. As no surfactants were involved, these nanoparticles were quickly built and spontaneously aggregated to minimize their surface area through the process known as Ostwald ripening.

The PANI/Bi_2WO_6 had shown the excellent photocatalytic performance on the degradation of the widely used dye and common indoor air pollution. It was film and suitable band gap that resulted the excellent photocatalytic efficiency. The photogenerated holes in VB can directly transfer to the π-orbital of PANI. Simultaneously, the photogenerated electrons can transfer to the CB of Bi_2WO_6, which results in charge separation and stabilization.

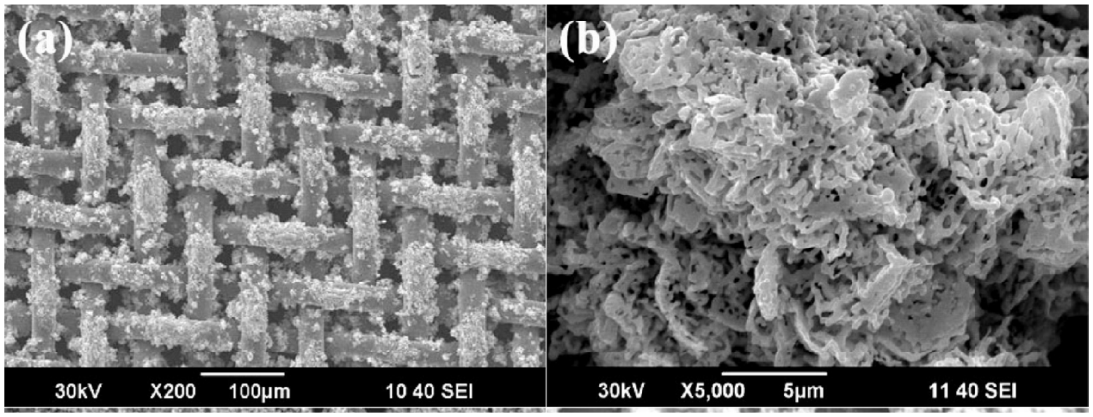

Figure 18: SEM images of as-synthesized Bi_2WO_6 films by CBD process at 5 mM concentrations of low (a) and high (b) magnifications.

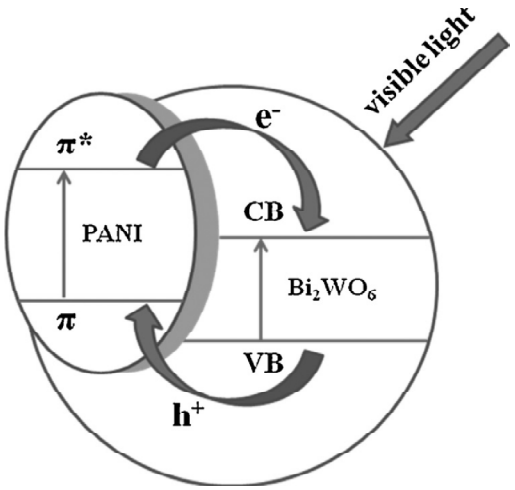

Figure 19: Schematic diagram for energy band matching and migration and separation of electron–hole pairs in the coupled PANI/Bi_2WO_6 system.

4.3. PANI/$BiVO_4$

Photocatalytic active spindle-like $BiVO_4$ modiûed by polyaniline (PANI) was synthesized via a sonochemical approach for the ûrst time [48]. From the SEM pattern (Fig. 20B), a close-up view of the spindles demonstrated that the majority of the crystals possess a uniform spindle-like shape with center diameter of about 400 nm and length of about 800 nm. At the same time, On the basis of the small grain size, the intrinsic property of PANI, and the synergic effect between PANI and $BiVO_4$, a rapid electron-hole separation and slow recombination came true. As a result, both the photodegradation of RhB and phenol with PANI-modified $BiVO_4$ photocatalysts under visible light ($\lambda > 420$ nm) were enhanced remarkably.

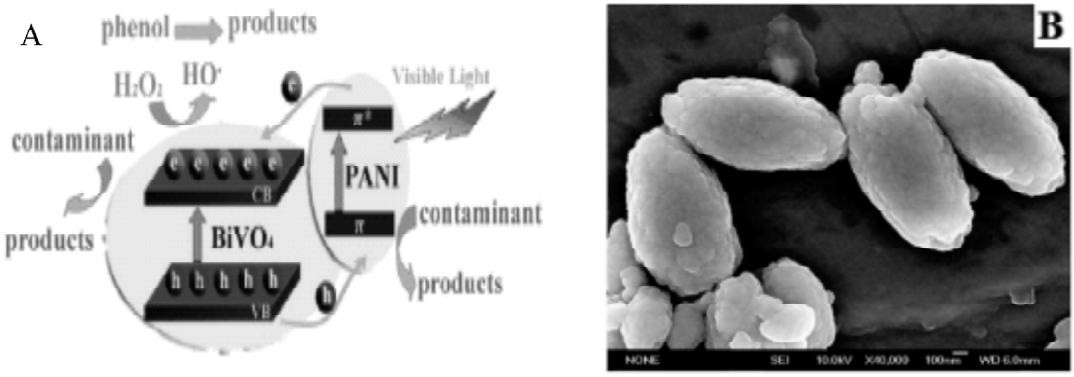

Figure 20: (A) Photocatalytic Mechanism for PANI/$BiVO_4$. (B) High-magniûcation SEM image of Spindle-like 0.5% PANI/$BiVO_4$ sample.

4.4. PANI /Bi_3NbO_7

Wu Ling and co-workers recently reported polyaniline/Bi_3NbO_7 nanocomposites prepared via a sol–gel method and simple chemisorption approach [49]. Due to the high efficiency of charge separation induced by the synergetic effect between PANI and Bi_3NbO_7 (Fig. 21), The photocatalytic activities of the as-prepared samples for the rhodamine B degradation demonstrated the samples exhibited excellent photocatalytic activities and high activity stabilities for the degradation of rhodamine B.

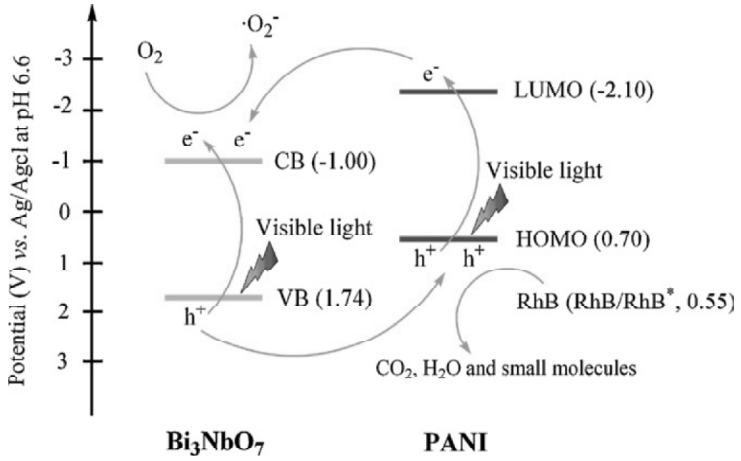

Figure 21: Probable degradation process of RhB over PANI/Bi_3NbO_7 nanocomposite.

5. g-C_3N_4-Bi based composite

Graphitic carbon nitride (g-C_3N_4) has high nitrogen content with excellent chemical and thermal stability. It was first reported by Wang et al. which applied in photocatalytic hydrogen production and photocatalytic degradation of organic pollutants [50].

5.1. g-C_3N_4- $BiPO_4$

Li zhesheng [51] recently reported that they had synthesized the novel hybrid architectures of $BiPO_4$ and mesoporous C_3N_4 as a composite photocatalyst for environmental application. The photocatalytic activity of the $BiPO_4/C_3N_4$ for degradation of Methyl Orange Dye has been significantly improved under visible-light irradiation (Fig. 22b).

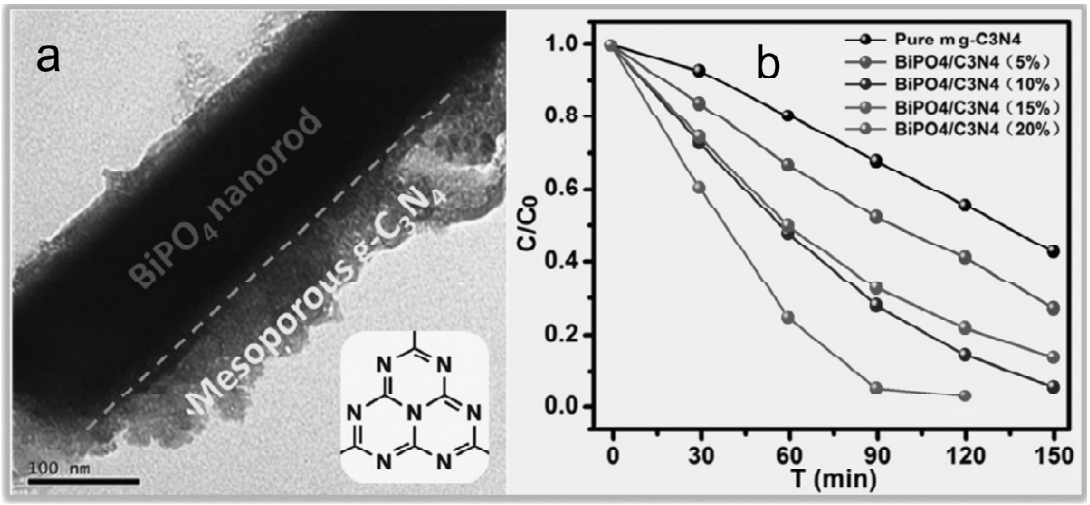

Figure 22: Typical TEM images of the as-prepared samples (a) and photocatalytic activities (b).

To show further insight into the excellent performances of the $BiPO_4$ NRs/mC_3N_4 composite photocatalyst, a mechanism was built to depict the main charge-transfer processes between $BiPO_4$ and C_3N_4 components (Fig. 23). Firstly, under visible-light irradiation, photogenerated electron–hole pairs were formed on g-C_3N_4. The electrons at the conduction band (CB) of C_3N_4 were injected into the CB of $BiPO_4$, thus promoting charge separation to enhance photocatalysis of C_3N_4. Secondly, the hydrogen ions which ionized from water molecular will combine with the moderate oxidant $\cdot O^-_2$ and one more e^- to form H_2O_2 molecular. H_2O_2 can then be further activated to the most reactive ·OH by accepting a third photo-induced electron and cause the formation of ·OH groups. Meanwhile, the holes on the valence band (VB) of $BiPO_4$ transferred to the surface of the C_3N_4, where more ·OH groups were generated, therefore leading to a much reduced electron–hole recombination and improved photocatalytic efficiency for MO degradation.

5.2. g-C_3N_4–BiOCl

Novel BiOCl–C_3N_4 heterojunctions were synthesized through an in situ ionic-liquid-assisted solvent-thermal method, through which a highly dispersed heterointerface was formed with almost no loss of C_3N_4 [52]. BiOCl was dispersed on C_3N_4 to form heterojunction structures with high specific surface area and the ability to absorb visible light (Fig. 24). The photocatalytic results for the degradation of methyl orange (MO) indicated that the most active heterojunction proportion is 1BiOCl:1C_3N_4, which increased

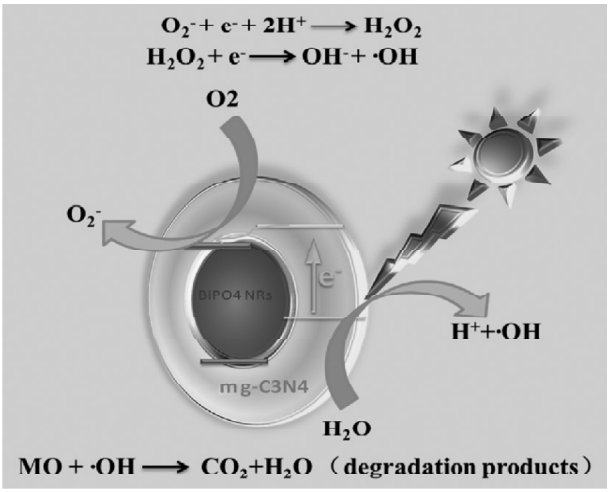

Figure 23: Schematic diagram for the charge separation in a visible light irradiated $BiPO_4/C_3N_4$ system.

the visible light photocatalytic activity 3.3-fold relative to that of a sample of the mechanically mixed counterpart of this composition (Fig. 25). A schematic diagram of the BiOCl–C_3N_4 heterojunctions was proposed on the basis of experimental and theoretical results. C_3N_4 absorbs visible light to induce π–π* transitions, which results in the transport of the excited-state electrons from the HOMO to the LUMO. The LUMO potential of C_3N_4 (_1.13 eV) is more negative than the conduction band (CB) edge of BiOCl (0.23 eV). Due to the well-aligned straddling band structures of BiOCl–C_3N_4 upon their intimately contacted interface, the excited electron on C_3N_4 could directly inject into the CB of BiOCl. $C_3N^+_4$ would accept electrons from fragments of MO degradation and return to the ground state. The electrons on the CB edge of BiOCl would subsequently transfer to the photocatalyst surface to react with the intermediate products of the degradation.

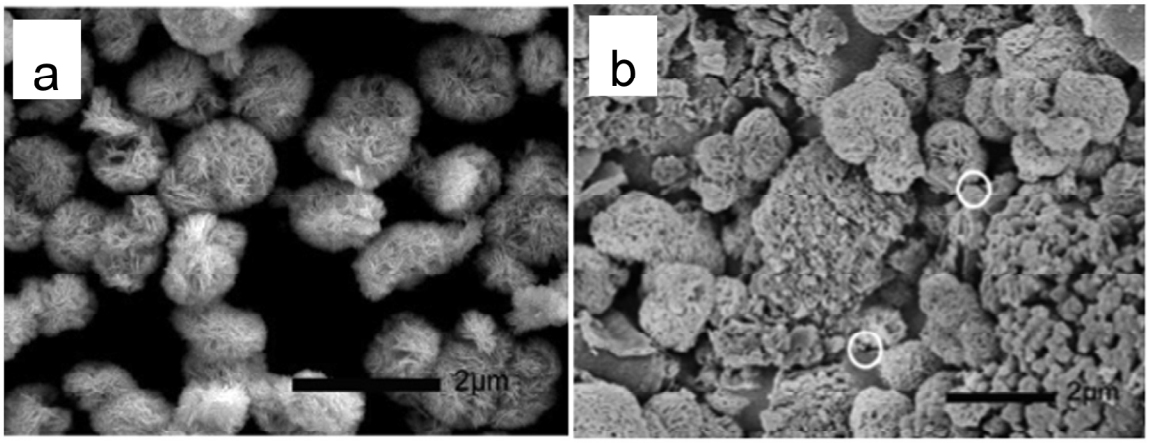

Figure 24:SEM images of (a) C_3N_4, (b) 1BiOCl–1C_3N_4 heterojunction samples.

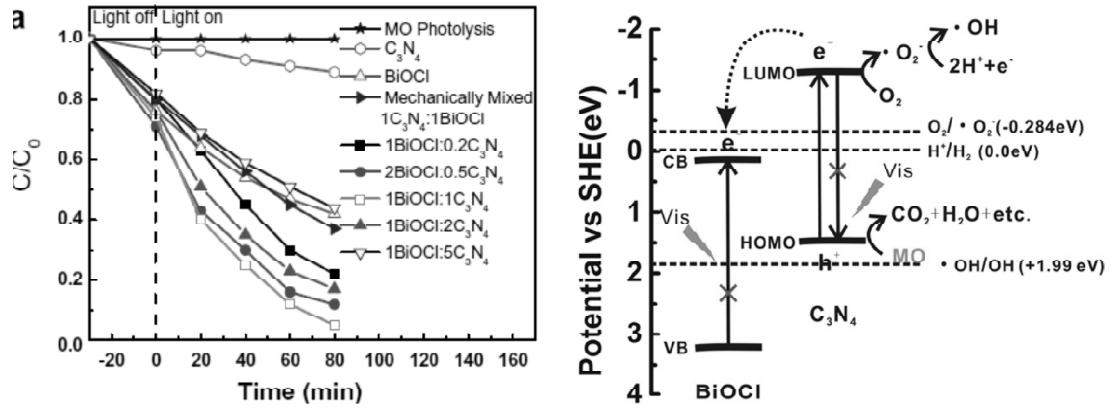

Figure 25: Photocatalytic activities of BiOCl, C_3N_4, and BiOCl–C_3N_4 samples on the degradation of MO under visible light irradiation and schematic diagram of the separation and transfer of photogenerated charges in the BiOCl–C_3N_4 heterojunctions combined with the possible reaction mechanism.

Shen kai and coworkers synthesized g-C_3N_4 modified BiOCl hybrid photocatalyst prepared through hydrolysis process of Bi^{3+} onto g-C_3N_4, using $NaBiO_3$ and g-C_3N_4 produced from pyrolysis of melamine as the starting materials [53]. They found that the photoactivity enhancement is strongly dependent on the active role played by the frontier orbital energy levels of dye molecules by Quantum chemical calculations and a probable correlation of structure–activity relationship was established. The mechanism of RhB is showed in Fig. 26, active radicals are the main active species which result the RhB decomposition.

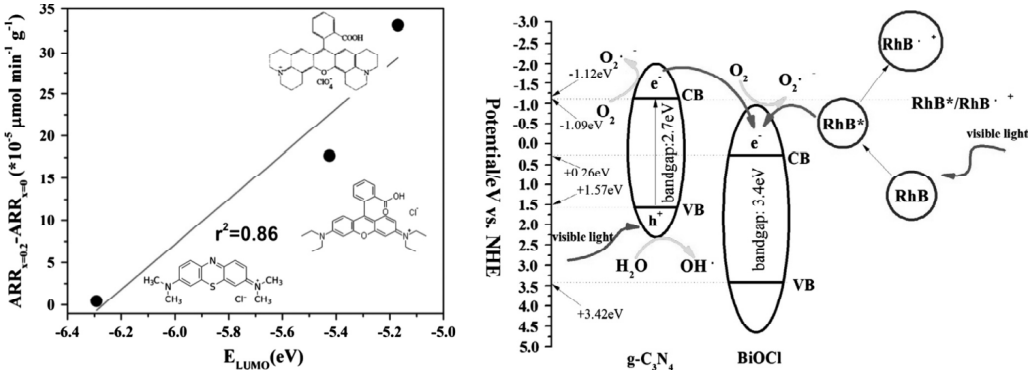

Figure 26: Relationship between the photodegradation enhancement and E_{LUMO} of Rh640, Rh B and MB and Proposed photodegradation mechanism of RhB on g-C_3N_4/BiOCl hybrid photocatalyst under visible light irradiation.

5.3. g-C_3N_4-Bi_2WO_6

The novel g-C_3N_4/Bi_2WO_6 heterostructured photocatalysts were prepared for the first time via mixing and heating methods by Ge Lei [54]. The results demonstrated that compared

with pure Bi_2WO_6 and g-C_3N_4, the g-C_3N_4/Bi_2WO_6 heterojunction photocatalyst had a remarkably enhanced MO photodegradation activity under visible light irradiation (Fig. 27). The electrons in Bi_2WO_6 crystals are good reductants that could capture the adsorbed O_2 onto the composite catalyst surface and reduce it to $O_2^{-\cdot}$ The highly oxidative species •OH is produced as a consequence of the reduction of oxygen. The photo-generated holes (h+) in g-C_3N_4 can also react with H_2O and cause the formation of •OH groups, leading to a constant stream of the surface •OH groups.

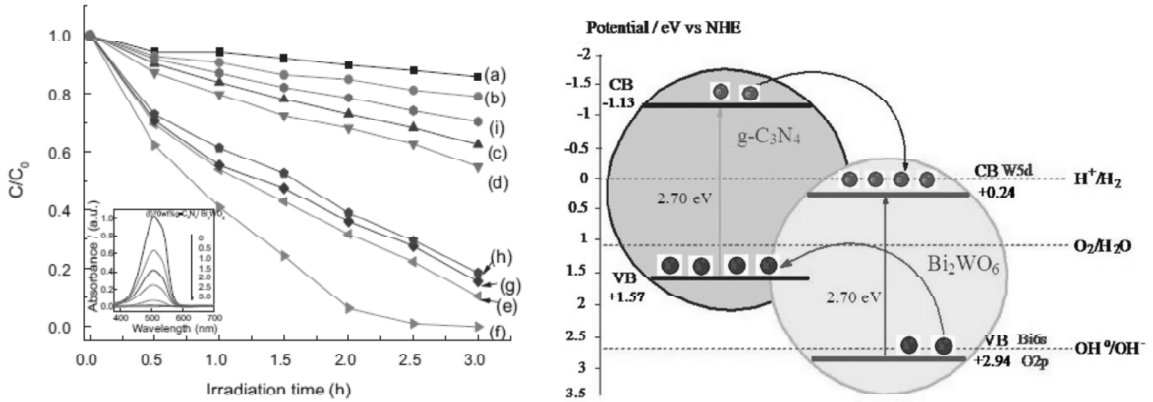

Figure 27: Degradation rates of methyl orange under visible light irradiation using (a) pure Bi_2WO_6, (h) pure g-C_3N_4, as well as g-C_3N_4/Bi_2WO_6 with different g-C_3N_4 concentrations of (b) 5.0 wt%, (c) 10.0 wt%, (d) 30 wt%, (e) 50 wt%, (f) 70 wt%, and (g) 90 wt% and diagrams of the energy position and photogenerated electron–hole pair transfers between polymeric g-C_3N_4 and Bi_2WO_6.

Wang Huihu and co-workers also synthesized g-C_3N_4/Bi_2WO_6 composites by directly introducing g-C_3N_4 powder to the Bi_2WO_6 precursor solution, which was then reacted in a hydrothermal environment [55]. The photocatalytic efficiency is much the same as the efficiency of what Ge Lei and co-workers had synthesized.

6. Summary and Outlook

Photocatalytic materials have a broad development potential in deep water purification and organic pollutant in air cleaning fields, which have drown more and more attention in recent several years. Figuring out the inner factors of influencing the efficiency of photocatalyst, promoting the separation of the charges to reduce the possibility of recombination, discovering the novel material system, increasing the superficial photocatalytic active sites, broadening the efficiency of solar spectrum, especially in visible light, improving oxidizing ability and designing high-efficiency photocatalytic reactors are our modified direction in the future. In these photocatalysts, bismuth-based with conjugated π molecule such as CNTs, graphene, PANI and g-C_3N_4 have drawn much attention due to their specific structures and excellent visible response. However, these photocatalysts also have fatal defects. For example, reuse, stability, solubleness and photocorrosion have not shown satisfactory results in these ways due to our impercipient

situation of photocatalytic mechanism. So there are a lot of works to do in photocatalytic field. Bismuth-based with conjugated π molecule composites should become the one of the most important photocatalytic materials by subsequent continuous study.

Acknowledgements

This work was financially supported by the National Science and Technology Support Project (Grant No. 2011BAJ03B04), Natural Science Foundation of China (Grant No. 21171004), and Natural Science Foundation of Anhui province (1408085MB33).

References

[1] J. L. Su, Y. Xiao, M. Ren, "Direct hydrolysis synthesis of BiOI flowerlike hierarchical structures and it is photocatalytic activity under simulated sunlight irradiation," *Catalysis Communications*, **45**: 30-33(2014).

[2] J. Zhang, F. J. Shi, J. Lin, D. F. Chen, J. M. Gao, Z. X. Huang, X. X. Ding, C. C. Tang, "Self-Assembled 3-D Architectures of BiOBr as a Visible Light-Driven Photocatalyst," *Chem. Mater*, **20**: 2937–2941 (2008).

[3] K. Zhang, J. Liang, S. Wang, J. Liu, K. X. Ren, X. Zheng, H. Luo, Y. J. Peng, X. Zou, X. Bo, J. H. Li, X. B. Yu, "BiOCl Sub-Microcrystals Induced by Citric Acid and Their High Photocatalytic Activities," *Crystal Growth and Design*, **12**: 793-803 (2012).

[4] R. Shi, G. L. Huang, J. Lin, Y. F. Zhu, "Photocatalytic Activity Enhancement for Bi_2WO_6 by Fluorine Substitution," *Journal of Physical Chemistry Communication*, **113**: 19633-19638 (2009).

[5] F. J. Zhang, F. Z. Xie, J. Liu, W. Zhao, K. Zhang, "Rapid sonochemical synthesis of irregular nanolaminar-like Bi_2WO_6 as efficient visible-light-active photocatalysts," *Ultrasonics Sonochemistry*, **20**: 209-215 (2013).

[6] L. Chen, S. F. Yin, S. L. Luo, R. Huang, Q. Zhang, T. Hong, Peter C.T. Au, "$Bi_2O_2CO_3$/BiOI Photocatalysts with Heterojunctions Highly Efficient for Visible-Light Treatment of Dye-Containing Wastewater," *Ind. Eng. Chem. Res.*, **51**: 6760–6768 (2012).

[7] S. Tokunaga, H. Kato, A. Kudo, "Selective Preparation of Monoclinic and Tetragonal $BiVO_4$ with Scheelite Structure and Their Photocatalytic Properties," *Chem. Mater.*, **13**: 4624–4628 (2001).

[8] X. Zhao, T. G. Xu, "Photodegradation of dye pollutants catalyzed by ã-Bi_2MoO_6 nanoplate under visible light irradiation," *Applied Surface Science*, **255**: 8036-8040 (2009).

[9] F. J. Zhang, S. F. Zhu, F. Z. Xie, J. Zhang, Z. D. Meng, "Plate-on-plate structured Bi_2MoO_6/Bi_2WO_6 heterojunction with high-efficiently gradient charge transfer for decolorization of MB," *Separation and Purification Technology*, **113**: 1-8 (2013).

[10] S. C. Yan, Z. S. Li, Z. G. Zou, "Photodegradation performance of g-C_3N_4 fabricated by directly heating melamine," *Langmuir*, **25**: 10397-10401 (2009).

[11] X. J. Bai, L. Wang, R. L. Zong, Y. F. Zhu, "Photocatalytic activity enhanced via g C_3N_4 nanoplates to nanorods," *The Journal of Physical Chemistry C*, **117**: 9952-9961 (2013).

[12] S. Cho, H. Jeong, D. H. Park, S. H. Jung, H. J. Kim, K. H. Lee, "The effects of vitamin C on ZnO crystal formation," *Cryst Eng Comm,* **12**: 968–976 (2010).

[13] S. Cho, J. W. Jang, J. S. Lee, K. H. Lee, "Carbon-doped ZnO nanostructures synthesized using vitamin C for visible light photocatalysis," *Cryst Eng Comm,* **12**: 3929–3935 (2010).

[14] H. Li, D. Wang, H. Fan, P. Wang, T. Jiang, T. Xie, "Synthesis of highly efficient C doped TiO_2 photocatalyst and its photo-generated charge-transfer properties," *Journal of Colloid and Interface Science*, **354**: 175–180 (2011).

[15] S. Iijima, "Helical microtubules of graphitic carbon," *Nature*, **354**: 56–58 (2010).

[16] C. Y. Nie, L. K. Pan, Y. Liu, H. B. Li, T. Q. Chen, T. Lu, Z. Sun, "Electrophoretic deposition of carbon nanotubes–polyacrylic acid composite ûlm electrode for capacitive deionization," *Electrochim. Acta,* **66**: 106–109 (2012).

[17] J. Yang, L. Zou, H. H. Song, "Preparing MnO_2/PSS/CNTs composite electrodes by layer-by-layer deposition of MnO_2 in the membrane capacitive deionisation," *Desalination*, **286**: 108–114 (2012).

[18] H. X. Zhao, H. F. Li, H. T. Yu, H. M. Chang, X. Quan, S. Chen, "CNTs–TiO_2/Al_2O_3 composite membrane with a photocatalytic function: Fabrication and energetic performance in water treatment," *Separation and Purification Technology*, **116**: 360-365 (2013).

[19] Y. Wang, H. Chang, H. Wu, H. Liu, "Bioinspired prospects of graphene: from biosensing to energy," *Journal of Materials Chemistry B*, **1**: 3521–3534 (2013).

[20] R. Rao, S. Singh, B. R. Singh, W. Khan, A. H. Naqvi, "Synthesis and characterization of surface modiûed graphene–zirconium oxide nanocomposite and its possible use for the removal of chlorophenol from aqueous solution," *Journal of Environmental Chemical Engineering*, **2**: 199-210 (2014).

[21] L. Zhang, F. Zhang, X. Yang, G. Long, Y. Wu, T. Zhang, K. Leng, Y. Huang, Y. Ma, A. Yu, Y. Chen, "Porous 3D graphene-based bulk materials with exceptional high surface area and excellent conductivity for supercapacitors," *Scientiûc Reports* **3** (2013).

[22] W. D. Wang, F. Q. Huang, X. P. Lin, "xBiOI–(1-x)BiOCl asefficient visible-light-driven photocatalysts," *Scripta Materialia*, **56**: 669 (2007).

[23] J. H. Yu, B. Wei, L. Zhu, H. Gao, W. J. Sun, L. L. Xu, "Flowerlike C-doped BiOCl nanostructures: Facile wet chemical fabrication and enhanced UV photocatalytic properties," *Applied Surface Science*, **284**: 497-502 (2013).

[24] J. X. Xia, J. Di, S. Yin, H. M. Li, L. Xu, Y. G. Xu, C. Y. Zhang, H. M. Shu, "Improved visible light photocatalytic activity of MWCNT/BiOBr composite synthesized via a reactable ionic liquid," *Ceramics International*, **40**: 4607-4616 (2014).

[25] Y. H. Lv , H. Liu, W. Zhang, S. L. Ran, F. L. Chi, B. Yang, A. L. Xia, "Room-temperature synthesis and high visible-light-induced photocatalytic activity of AgI/BiOI composites," *Journal of Environmental Chemical Engineering*, **1**: 526-533 (2013).

[26] L. Ge, C. C. Han, "Synthesis of MWNTs/g-C_3N_4 composite photocatalysts with efûcient visible light photocatalytic hydrogen evolution activity," *Applied Catalysis B: Environmental*, 117-118: 268-274 (2012).

[27] H. X. Shi, J. Y. Chen, G. Y. Li, X. Nie, H. J. Zhao, P. K. Wong, T. C. An, "Synthesis and Characterization of Novel Plasmonic Ag/AgX-CNTs (X= Cl, Br, I) Nanocomposite Photocatalysts and Synergetic Degradation of Organic Pollutant under Visible Light," *Acs Applied Materials and Interfaces*, **5**: 6959-6967 (2013).

[28] H. Z. Chen, S. G. Yang, K. Yu, Y. M. Ju, C. Sun, "Effective Photocatalytic Degradation of Atrazine over Titania-Coated Carbon Nanotubes (CNTs) Coupled with Microwave Energy," *The Journal of Physical Chemistry A*, **115**: 3034-3041 (2011).

[29] F. J. Zhang, W. C. Oh, K. Zhang, "New insight for enhancing photocatalytic activity of MWCNT/TiO_2 by decorating palladium nanoparticles as charge-transfer channel," *Materials Research Bulletin*, **47**: 619-624 (2012).

[30] M. H. Su, C. He, L. F. Zhu, Z. J. Sun, C. Shan, Q. Zhang, D. Shu, R. L. Qiu, Y. Xiong, "Enhanced adsorption and photocatalytic activity of BiOI–MWCNT composites towards organic pollutants in aqueous solution," *Journal of Hazardous Materials*, 229-230: 72-82 (2012).

[31] Y. Yan, S. F. Sun, Y. Song, X. Yan, W. S. Guan, X. L. Liu, W. D. Shi, "Microwave-assisted in situ synthesis of reduced graphene oxide-$BiVO_4$ composite photocatalysts and their enhanced photocatalytic performance for the degradation of ciprofloxacin," *Journal of Hazardous Materials*, 250-251: 106-114 (2013).

[32] J. Meyer, A.Geim, M. Katsnelson, K. Novoselov, T. Booth, S. Roth, "The Structure of Suspended Graphene Sheets," *Nature*, 446: 60–63 (2007).

[33] J. S. Bunch, A. M. van der Zande, S. S. Verbridge, I. W. Frank, D. M. Tanenbaum, J. M. Parpia, H. G. Craighead, P. L. McEuen, "Electromechanical Resonators from Graphene Sheets," *Science*, 315: 490–493 (2007).

[34] H. Liu, Y. Su, Z. Chen, Z. T. Jin, Y. Wang, "Graphene sheets grafted three-dimensional $BiOBr_{0.2}I_{0.8}$ microspheres with excellent photocatalytic activity under visible light," *Journal of Hazardous Materials*, 266: 75-83 (2014).

[35] X. M. Zhang, X. F. Chang, M.A. Gondal, B. Zhang, Y. S. Liu, G. B. Ji, "Synthesis and photocatalytic activity of graphene/BiOBr composites under visible light," *Applied Surface Science*, **258**: 7826-7832 (2012).

[36] J. Y. Liu, Y. Bai, P. Y. Luo, P. Q. Wang, "One-pot synthesis of graphene–BiOBr nanosheets composite for enhanced photocatalytic generation of reactive oxygen species," *Catalysis Communications*, **42**: 58-61 (2013).

[37] Y. K. Li, S. Y. Dong, Y. F. Wang, J. Y. Sun, Y. F. Li, Y. Q. Pi, L. M. Hu, J. H. Sun, "Reduced graphene oxide on a dumbbell-shaped $BiVO_4$ photocatalyst for an augmented natural sunlight photocatalytic activity," *Journal of Molecular Catalysis A: Chemical*, **387**: 138-146 (2014).

[38] Y. S. Fua, X. Q. Sun, X. Wang, "$BiVO_4$–graphene catalyst and its high photocatalytic performance under visible light irradiation," *Materials Chemistry and Physics*, **131**: 325-330 (2011).

[39] H. Liu, W. R. Cao, Y. Su, Z. Chen, Y. Wang, "Bismuth oxyiodide–graphene nanocomposites with high visible light photocatalytic activity," *Journal of Colloid and Interface Science*, **398**: 161-167 (2013).

[40] W. D. Zhang, F. Dong, T. Xiong, Q. Zhang, "Synthesis of BiOBr–graphene and BiOBr–graphene oxide nanocomposites with enhanced visible light photocatalytic performance," *Ceramics International*, 01: 112 (2014).

[41] H. W. Ma, J. F. Shen, M. Shi, X. Lu, Z. Q. Li, Y. Long, N. Li, M. X. Ye, "Significant enhanced performance for Rhodamine B, phenol and Cr(VI) removal by Bi_2WO_6 nancomposites via reduced graphene oxide modification," *Applied Catalysis B: Environmental*, 121-122: 198-205 (2012).

[42] J. J. Xu, Y. H. Ao, M. D. Chen, "A simple method for the preparation of Bi_2WO_6-reduced graphene oxide with enhanced photocatalytic activity under visible light irradiation," *Materials Letters*, **92**: 126-128 (2013).

[43] Y. L. Min, K. Zhang, Y. C. Chen, Y. G. Zhang, "Enhanced photocatalytic performance of Bi_2WO_6 by graphene supporter as charge transfer channel," *Separation and Purification Technology*, 86: 98-105 (2012).

[44] S. E. Shaheen, C. J. Brabec, F. Padinger, T. Fromherz, J. C. Hummelen, N. S. Sariciftci, "2.5% efficient organic plastic solar cells," *Appl. Phys. Lett.* **78**: 841 (2001).

[45] E. T. Kang, K. G. Neoh, K. L. Tan, "Polyaniline: a polymer with many interesting intrinsic redox states," *Prog. Polym. Sci.* **23**: 277–324 (1998).

[46] Q. Z. Wang, J. Hui, J. J. Li, Y. X. Cai, S. Q. Yin, F. P. Wang, B. T. Su, "Photodegradation of methyl orange with PANI-modified BiOCl photocatalyst under visible light irradiation," *Applied Surface Science*, **283**: 577-583 (2013).

[47] W. Z. Wang, J. H. Xu, L. Zhang, S. M. Sun, "Bi_2WO_6/PANI: An efficient visible-light-induced photocatalytic composite," *Catalysis Today*, **224**: 147-153 (2014).

[48] M. Shang, W. Z. Wang, S. M. Sun, J. Ren, L. Zhou, L. Zhang, "Efficient Visible Light-Induced Photocatalytic Degradation of Contaminant by Spindle-like PANI/$BiVO_4$," *Journal of Physical Chemistry: C*, **113**: 20228-20233 (2009).

[49] W. M. Wu, S. J. Liang, L. J. Shen, Z. X. Ding, H. R. Zheng, W. Y. Su, L. Wu, "Preparation, characterization and enhanced visible light photocatalytic activities of polyaniline/Bi_3NbO_7 nanocomposites," *Journal of Alloys and Compounds*, **520**: 213-219 (2012).

[50] Y. Zheng, J. Liu, J. Liang, M. Jaroniec, S. Z. Qiao, "Graphitic carbon nitride materials: controllable synthesis and applications in fuel cells and photocatalysis," *Energy Environ. Sci.* **5**: 6717–6731 (2012).

[51] Z. S. Li, S. Y. Yang, J. M. Zhou, D. H. Li, X. F. Zhou, C. Y. Ge, Y. P. Fang, "Novel mesoporous g-C_3N_4 and $BiPO_4$ nanorods hybrid architectures and their enhanced visible-light-driven photocatalytic performances," *Chemical Engineering Journal*, **241**: 344-351 (2014).

[52] X. J. Wang, Q. Wang, F. T. Li, W. Y. Yang, Y. Zhao, Y. J. Hao, S. J. Liu, "Novel BiOCl-C_3N_4 heterojunction photocatalysts: In situ preparation via an ionic-liquid-assisted solvent-thermal route and their visible-light photocatalytic activities," *Chemical Engineering Journal,* **234**: 361-371 (2013).

[53] S. Shi, M. A. Gondal, A. A. Al-Saadi, R. Fajgar, J. Kupcik, X. F. Chang, K. Shen, Q. Y. Xu, Z. S. Seddigi, "Facile preparation of g-C_3N_4 modified BiOCl hybrid photocatalyst and vital role of frontier orbital energy levels of model compounds in photoactivity enhancement," *Journal of Colloid and Interface Science*, **416**: 212-219 (2014).

[54] L. Ge, C. C. Han, J. Liu, "Novel visible light-induced g-C_3N_4/Bi_2WO_6 composite photocatalysts for efficient degradation of methyl orange," *Applied Catalysis B: Environmental*, 108-109: 100-107 (2011).

[55] H. H. Wang, J. Lu, F. Q. Wang, W. H. Wei, Y. Chang, S. J. Dong, "Preparation, characterization and photocatalytic performance of g-C_3N_4/Bi_2WO_6 composites for methyl orange degradation," *Ceramics International*, **121**: 0272-8842 (2014).